RESEARCH ARTICLE | JANUARY 03 2023

Hybrid simulations of the decay of reconnected structures downstream of the bow shock

I. Gingell ✉; S. J. Schwartz; H. Kucharek; ... et. al

Physics of Plasmas 30, 012902 (2023)
https://doi.org/10.1063/5.0129084

Physics of Plasmas ARTICLE scitation.org/journal/php

Hybrid simulations of the decay of reconnected structures downstream of the bow shock

Cite as: Phys. Plasmas **30**, 012902 (2023); doi: 10.1063/5.0129084
Submitted: 3 October 2022 · Accepted: 28 November 2022 ·
Published Online: 3 January 2023

I. Gingell,[1,a)] S. J. Schwartz,[2] H. Kucharek,[3] C. J. Farrugia,[3] L. J. Fryer,[1] J. Plank,[1] and K. J. Trattner[2]

AFFILIATIONS

[1]School of Physics and Astronomy, University of Southampton, Southampton SO17 1BJ, United Kingdom
[2]Laboratory for Atmospheric and Space Physics, University of Colorado, Boulder, Colorado 80303, USA
[3]Space Science Center, University of New Hampshire, Durham, New Hampshire 03824, USA

[a)]Author to whom correspondence should be addressed: i.l.gingell@soton.ac.uk

ABSTRACT

Observations by Magnetospheric Multiscale have demonstrated that magnetic reconnection occurs at Earth's bow shock, typically at thin current sheets arising from plasma instabilities and turbulence in the shock transition region. Observational surveys of both the shock transition and the magnetosheath downstream suggest that the number of current sheets in these regions may not be strongly dependent on the shock Mach number M_A or the angle between the upstream magnetic field and shock normal (θ_{Bn}). This result is somewhat surprising given that quasi-parallel and high Mach number shocks tend to have a more disordered and non-stationary structure. In order to investigate how shock reconnection manifests across different parameters, we perform a series of hybrid (fluid electron, kinetic ion) particle-in-cell simulations across a range of Mach numbers and orientations. Given that hybrid simulations cannot resolve electron-scale current sheets and reconnection, these simulations isolate an ion-scale mechanism for shock reconnection driven by an ion–ion beam instability in the foot. We find that this mechanism is strongly constrained to quasi-parallel shocks across all simulated Mach numbers. By quantifying reconnection using the area occupied by plasma on closed magnetic field lines, we find the number of reconnecting structures and closed field area increase with M_A and decrease with θ_{Bn} in the upstream and ramp regions. Downstream of the shock, however, we find a similar result to observational surveys: within the subset of quasi-parallel shocks, the decay rate of the closed field area (and hence thin current sheets) is not strongly dependent on upstream shock parameters.

I. INTRODUCTION

Collisionless shock waves are ubiquitous across diverse astrophysical and space plasma environments, including stellar and planetary bow shocks, interplanetary shocks in the solar wind, and supernova remnants.[1] In crossing the shock wave, the bulk flow of the plasma is reduced from supersonic to sub-sonic speeds. Energy in the bulk flow is dissipated by means of "kinetic" plasma processes involving the direct interaction of the ions and electrons with the electromagnetic fields. Understanding which microphysical processes contribute to energy re-partition, and how, is critical for characterizing particle heating and acceleration at collisionless shocks.[2–4] However, the balance of kinetic phenomena involved in this process is strongly dependent on shock parameters such as the fast magnetoacoustic Mach number M_{fast}, the Alfvén Mach number M_A, the plasma beta β, and the angle between the upstream magnetic field and the shock surface normal θ_{Bn}.[1]

Recent observations by the Magnetospheric Multiscale (MMS) spacecraft have established that magnetic reconnection, a localized change in magnetic topology, which leads to transfer of energy from electromagnetic fields to particles, occurs at thin current sheets within the transition region of Earth's bow shock.[5,6] The transition region in this case extends from the shock foot upstream to the downstream region behind the shock ramp. These initial case studies included observations of actively reconnecting, thin current sheets in the transition regions of both quasi-parallel ($\theta_{Bn} < 45°$) and quasi-perpendicular ($\theta_{Bn} > 45°$) shocks, demonstrating that reconnecting structures can be associated with a broad range of shock orientations. Furthermore, these case studies also included observations of thin current sheets which exhibit "electron-only" reconnection, for which only electron outflows are seen without associated ion outflows. Electron-only reconnection has been previously observed occurring at thin current sheets associated with magnetosheath turbulence.[7,8] A statistical

survey of active magnetic reconnection sites in the shock transition[9] has also established that reconnection is common at Earth's bow shock, evident in ∼40% of bow shock crossings observed by MMS, across all bow shock parameters. Quasi-parallel and high Mach number shocks were only weakly over-represented in the population of shock crossings exhibiting reconnection. Of most relevance to the following study, 88% of the reconnection sites were observed in the transition region downstream of the shock ramp, with fewer appearing deeper into the magnetosheath. The decay of the prevalence of current sheets downstream of the shock was also seen in a survey of thin current sheets in the magnetosheath.[10] The presence of reconnecting current sheets in the shock transition, therefore, implies that reconnection may play a role in the re-partition of energy across collisionless shock waves. However, the total impact is not yet known. An analysis of the energetics of thin current sheets downstream of a quasi-parallel bow shock observed by MMS[11] revealed that, for that single crossing, approximately ∼10% of the solar wind ram energy was processed at thin current sheets.

Simulations of reconnection within the shock transition region have revealed several mechanisms at play, dependent upon the parameters of each given shock. For the case of perpendicular, high Mach number shocks, Matsumoto *et al.*[12] demonstrated that reconnection can occur at filaments in the shock foot generated by the ion Weibel instability, leading to the development of several magnetic islands along each filament. This instability is expected to affect the shock structure significantly for Alfvén and fast magnetoacoustic Mach numbers in excess of $\sim 20-40$.[13] For quasi-parallel shocks with Mach numbers more typical of Earth's bow shock (i.e., $M_A \sim 8$), Gingell *et al.*[14] demonstrated the generation of magnetic islands via reconnection as a result of steepening of ion-scale waves in the shock foot. This process was shown to be modulated by cyclic reformation of the shock ramp. The underlying mechanism was investigated in more detail by Bessho *et al.*,[15] who attributed the ion-scale waves to the non-resonant ion–ion beam instability.[16] This ion–ion beam instability derives from the interaction of the incident, solar wind ions and the back-streaming ions reflected during their interaction with the shock. This instability excites ultra-low frequency (ULF) waves in the region upstream of the shock, typically with wavelengths on the order of 10 to dozens of ion inertial lengths. These waves steepen and bend the magnetic field lines, resulting in magnetic reconnection between adjacent wave crests. Furthermore, Bessho *et al.*[16] identified a secondary instability of the electron outflows associated with shorter wavelength whistler waves. Many of the reconnection sites generated by this secondary mechanism are examples of electron-only reconnection,[17] as described for magnetosheath turbulence by Phan *et al.*[7] With an extension to three dimensions, Ng *et al.*[18] showed that without the constraints of the 2D geometry, a range of guide fields and current sheet orientations are possible. Finally, we note that reconnection within the turbulent or disordered shock transition region has also been observed within low-β, quasi-perpendicular shock simulations by Lu *et al.*,[19] for which the Mach number was again typical of Earth's bow shock. Thus, as with observational surveys of shocks, simulations have shown that shock-driven reconnection appears across a broad range of scales and shock parameters.

Together these observational and numerical studies establish that reconnection can occur in the shock transition region by several mechanisms across a broad parameter space. In addition, the prevalence of reconnected structure may not be strongly dependent on shock orientation θ_{Bn} despite the quasi-parallel shock and magnetosheath typically exhibiting more disordered or turbulent structure. Hence, a broad parametric study is necessary to establish how reconnection manifests in different parameter regimes, and how the downstream magnetosheath responds in each case. This will enable us to better characterize energy transfer and dissipation at the shock and in magnetosheath turbulence.

In this paper, we address the parametric dependence of magnetic reconnection at the bow shock by means of a family of hybrid particle-in-cell codes. In Sec. III B, we introduce a method to quantify the impact of magnetic reconnection on the magnetic structure in and around the shock by measuring the area of closed magnetic field structures present within the simulations. We thereby assess the prevalence of structures associated with the shock-driven reconnection as a function of time and distance from the shock. In Sec. III C, we examine the differences in the closed-field area (and hence reconnection) observed between different shock parameters. Most importantly, we find that the decay of reconnected magnetic structure downstream of quasi-parallel shocks is not strongly dependent on the shock Mach number or orientation θ_{Bn}.

II. SIMULATION MODEL

For this study, we perform a series of hybrid particle-in-cell simulations[20] over a range of shock parameters. The chosen hybrid model combines a fully kinetic, particle-in-cell treatment of the ions with a charge-neutralizing, massless and isothermal electron fluid. The electromagnetic fields and moments are advanced using Maxwell's equations in the low-frequency limit, implemented using the current advance method and cyclic leapfrog (CAM-CL) algorithm described by Matthews.[21] This code is otherwise adapted from the fully kinetic particle-in-cell code EPOCH.[22] The use of a hybrid code for this study confers two important benefits: (i) we capture the continuing evolution of ion-scale structure far downstream of the shock over hundreds of ion inertial lengths, without the high computational cost of fully kinetic particle-in-cell models, and (ii) we are able to isolate and characterize the effects of ion-scale mechanisms for shock reformation, such as the ion–ion beam instability identified by Bessho *et al.*[16]

The simulations use a 2D grid in (x, y) comprising $(N_x, N_y) = (1600, 160)$ grid cells, with domain size $(L_x, L_y) = (240, 24)d_i$. The ion inertial length d_i is given by $d_i = V_A/\Omega_i$, where the Alfvén speed V_A and ion cyclotron frequency Ω_i are calculated in the undisturbed upstream region. The spatial resolution of the grid is, therefore, $\Delta x = \Delta y = 0.15d_i$. For a typical number density increase in four times in the downstream, shocked plasma, the downstream ion inertial length $d_{i,down} \approx 0.5d_i$. Hence, $\Delta x \approx 0.3d_{i,down}$ and $L_x \approx 480d_{i,down}$. The simulations discussed here are "2.5D," such that all three components of the electromagnetic fields and particle moments may vary on the two-dimension grid, e.g., $B_{x,y,z}(x, y, t)$. In the generalized Ohm's law we have used resistivity $\eta = 10^{-3}\mu_0 V_A^2/\Omega_i$. This parameter is chosen to ensure numerical stability of the model. Distance and time are normalized to the upstream ion inertial length and ion cyclotron frequency, and hence, velocities are normalized to the upstream Alfvén speed. The upper and lower boundaries at $y = 0, L_y$ are periodic, the boundary at $x = L_x$ is reflecting, and the boundary at $x = 0$ serves as a source for inflowing solar wind plasma. The initial conditions are homogeneous with number density $n = n_0$, magnetic field

$\mathbf{B} = B_0[-\cos(\theta_{Bn}), \sin(\theta_{Bn}), 0]$, and bulk inflow velocity $\mathbf{V} = [U_0, 0, 0]$. The interaction of the solar wind inflow in the $+x$-direction with the reflecting boundary at $x = L_x$ generates a shock moving in the $-x$-direction, with shock speed v_{sh} typically 1.5 to 2 V_A depending upon the initial conditions. The ions and electron fluid are initialized with plasma beta $\beta = 1$. The temperature of the inflowing solar wind plasma is fully determined by these initial conditions, giving $T_0 = \beta B_0^2/2\mu_0 n_0 k_B$. In order to reduce the noise as far as possible given the constraints of the available computational resources, the ion phase space has been sampled with 100 pseudo-particles per computational cell.

These simulations are performed for 22 individual cases over a range of inflow speeds $U_0/V_A = 2 - 12$ and magnetic field angles $\theta_{Bn} = 10°$–$70°$. As discussed later, we observe little or no reconnection at quasi-perpendicular shocks in this parameter range for this simulation model. Hence, we have not included shocks with $\theta_{Bn} > 70°$ in this paper. The full list of simulations and shock parameters, including the fast magnetoacoustic Mach number M_{fast}, is given in Table I. We refer to each simulation by the ID given in Table I, formed from a combination of the inflow speed U_0 and orientation θ_{Bn}.

III. RESULTS

Here, we discuss the evolution of the shock transition region, discuss a method for quantification of the prevalence of magnetic reconnection in the simulations, and explore the dependence of those measures on shock parameters.

TABLE I. Shock parameters for the simulations included in this study.

ID	U_0/V_A	v_{sh}/V_A	M_A	M_{fast}	$\theta_{Bn}(°)$
U2T10	2.0	−0.5	2.5	1.9	10
U3T10	3.0	−0.8	3.8	2.9	10
U3T20	3.0	−0.9	3.9	2.9	20
U3T30	3.0	−1.0	4.0	2.9	30
U3T40	3.0	−1.1	4.1	2.9	40
U3T50	3.0	−1.3	4.3	2.9	50
U6T10	6.0	−1.3	7.3	5.6	10
U6T20	6.0	−1.4	7.4	5.5	20
U6T30	6.0	−1.5	7.5	5.4	30
U6T40	6.0	−1.6	7.6	5.3	40
U6T50	6.0	−2.0	8.0	5.4	50
U6T60	6.0	−2.3	8.3	5.5	60
U6T70	6.0	−2.4	8.4	5.4	70
U9T20	9.0	−2.1	11.1	8.3	20
U9T30	9.0	−1.9	10.9	7.9	30
U9T40	9.0	−1.9	10.9	7.6	40
U9T50	9.0	−2.8	11.8	8.0	50
U9T60	9.0	−3.1	12.1	8.0	60
U12T30	12.0	−2.2	14.2	10.3	30
U12T40	12.0	−2.6	14.6	10.2	40
U12T50	12.0	−3.5	15.5	10.5	50
U12T60	12.0	−4.0	16.0	10.5	60

A. Evolution

The evolution of the magnetic structure in the shock transition region is shown for three different cases in Fig. 1. The plots each show the in-plane magnetic field lines with the out-of-plane magnetic field in color at three different times (from top to bottom), where each panel is approximately an ion gyroperiod advanced in time. The first two columns represent quasi-parallel ($\theta_{Bn} = 40°$) and quasi-perpendicular ($\theta_{Bn} = 60°$) cases for a typical Earth-like bow shock Mach number ($M_A \approx 8$), simulations U6T40 and U6T60, respectively. The third column shows the evolution of a higher Mach number $M_A \approx 15$ quasi-parallel shock with $\theta_{Bn} = 40°$, simulation U12T40. In this and future figures, the x-coordinate has been shifted by the position of the shock ramp $x_{sh}(t)$ such that the shock remains centered at $(x - x_{sh}) = 0$. The shock velocity in the simulation frame, and hence the position of the ramp $x_{sh}(t)$, is determined by the averaged behavior of the shock over the full period of the simulation. The true shock ramp may, therefore, deviate from x_{sh} over short time scales, reflecting non-stationarity in the transition region.

The left column of Fig. 1, showing simulation U6T40, clearly demonstrates the variability of the shock structure over ion timescales. We note in the upper panel the growth of ion-scale upstream waves associated with the non-resonant ion–ion beam instability,[23] driven by the interaction of the inflowing solar wind ions with the back-streaming ions. The growth of this instability, and the characteristics of these waves, is described in detail by Bessho *et al.*[16] In the second and third panels, the growth of these waves can be seen to lead to the generation of a disordered or turbulent transition region, exhibiting reconnecting current sheets and magnetic islands, as discussed for prior simulations in a similar parameter regime.[14,15] In subsequent panels, we observe the growth of a new shock ramp and its shock-wards propagation, consistent with a reformation cycle driven by the back-streaming ions (also seen in in Gingell *et al.*[14]). In the higher Mach number case U12T40 (right column), we also see evidence of the generation of a turbulent transition region. As in the $M_A \sim 8$ case shown in the left column, waves are excited in the upstream by an ion–ion beam instability driven by the interaction of the backstreaming, reflected ion population and the inflowing ions. However, in this high Mach number case, for which $M_A \sim 15$, the wavelength and amplitude of the excited upstream waves are larger: $\lambda \sim 3d_i$ for $M_A \sim 8$, and $\lambda \sim 10d_i$ for $M_A \sim 15$. This, in turn, leads to a more turbulent or disordered upstream region compared to the lower Mach number cases. This same difference between medium and high Mach number cases was observed for fully kinetic simulations of shocks in this parameter regime by Bessho *et al.*[16] A full dispersion analysis of the ion–ion beam instability observed here is beyond the scope of this paper and may be conducted as part of future investigations of the evolution of the turbulent transition region.

In the quasi-perpendicular case U6T60 (middle column), we do not observe upstream waves or significant out-of-plane magnetic fluctuations. Furthermore, we do not observe any shock reformation cycle; the upstream field is steady, and the shock ramp is most closely aligned with $x - x_{sh}(t) = 0$ throughout the interval shown. However, we do note that the shock surface appears to be rippled,[24–26] with a wavelength of approximately $5d_i$.

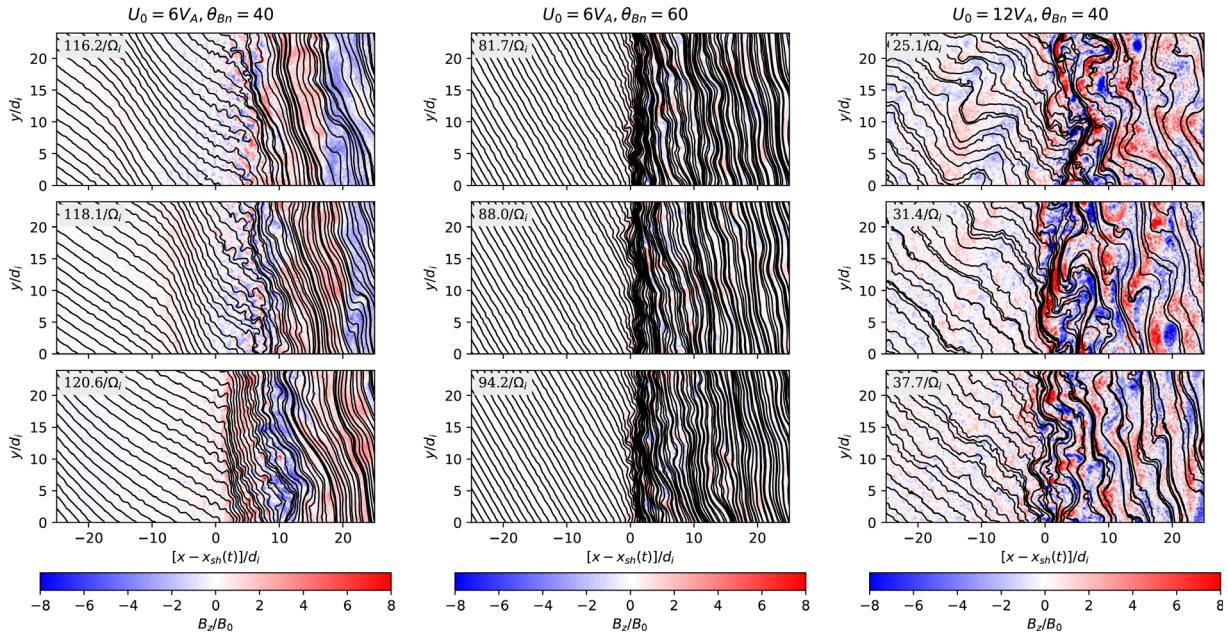

FIG. 1. Evolution of the magnetic field lines (black) and out-of-plane magnetic field $B_z(x, y)$ (color) at the shock over several ion-gyrotimes. Each column corresponds to a simulation from left to right as follows: U6T40, U6T60, and U12T40. The quasi-parallel simulations (left and right columns) demonstrate cyclic reformation of the shock structure and the periodic generation of a turbulent or disordered transition region hosting several magnetic islands.

B. Quantifying reconnection

In order to quantify how much reconnection has influenced the magnetic structure within a simulation at a given time, we examine the topology of the magnetic field lines within the 2D simulation plane. Specifically, we integrate magnetic field lines from the inflow boundary at $x = 0$ until they intersect the reflecting boundary at $x = L_x$, allowing for crossing of the periodic boundaries at $y = 0, L_y$. The field line starting points are evenly distributed along the inflow boundary $x = 0$ with sub-grid separation $0.2\Delta y$ (i.e., five field lines per grid cell). Finally, we labeled any simulation grid cell that is intersected by at least one of the integrated magnetic field lines as an "open field" region. Equivalently, any grid cell that is not crossed by any of the integrated field lines is a "closed field" region. An example of the output of this process is shown in Fig. 2, panel (a), which shows a subset of the integrated field lines (black) and the closed field regions (red) for simulation U6T40 with $M_A = 7.5$ and $\theta_{Bn} = 30°$. We find that this method clearly identifies regions of the disordered or turbulent shock transition region that have been closed as a result of magnetic reconnection. We note that a significant depletion in magnetic field strength may result in a misclassification of an area as "closed" if the reduction in field strength is greater than the typical number of field lines, we integrate per grid cell (i.e., $B/B_0 < 1/5$). These reductions may occur within foreshock structures such as short large-amplitude magnetic structures (SLAMSs).[27,28] We find that fewer than 3% of grid cells identified as closed also meet the threshold for problematic magnetic field strength depletions $B/B_0 < 1/5$. Additionally, these few grid cells are typically associated with the boundaries of larger closed field structures. Hence, potentially misclassified magnetic depletions are considered to be negligible for this study.

We examine the time evolution of the area of the closed field regions of the simulation, $A_{\text{closed}}(x, t)$, in panel (b) of Fig. 2. To generate this panel, we sum the number of closed field grid cells over the y-direction at every available position in x, for every available time. We note two key features of this panel. First, we observe a periodic appearance and disappearance of closed field regions within the shock ramp at $(x - x_{sh}) \approx 0$. This is a result of the modulation of the structure of the disordered transition region over ion timescales, associated with cyclic reformation of the shock.[14] Second, we observe that a significant closed field area is transmitted to the downstream region, visible as diagonal black bands within the region $(x - x_{sh}) > 0$. We see a gradual decay of the closed field area along these bands as the plasma convects further downstream of the shock.

Finally, we take the average of the distributions of closed field area $A_{\text{closed}}(x, t)$ for all times to arrive at a time-independent distribution of closed field area $\bar{A}_{\text{closed}}(x)$, shown as a blue line in panel (c) of Fig. 2. This effectively smooths out the influence of periodic shock reformation. As an additional measure, the red line in panel (c) represents the time-averaged distribution of the number of distinct closed field regions $\bar{N}_{\text{structures}}$, which have an area of at least 10 grid cells $(0.225d_i^2)$. Importantly, these time averages are performed only over the period during which the shock and upstream structure are well developed. To allow for the shock and foreshock to form, the average is taken only for $t\Omega_i > 20$. Similarly, the behavior of the shock may change as it comes close to the upstream boundary due to the loss of back-streaming ions in the foreshock. This effect is most clear in the quasi-parallel cases as a change or loss of the shock reformation cycle. Hence, the upper bound for the time averages is set individually for each simulation where we observe changes in behavior of the shock. For typical quasi-parallel shocks, this change occurs when the shock

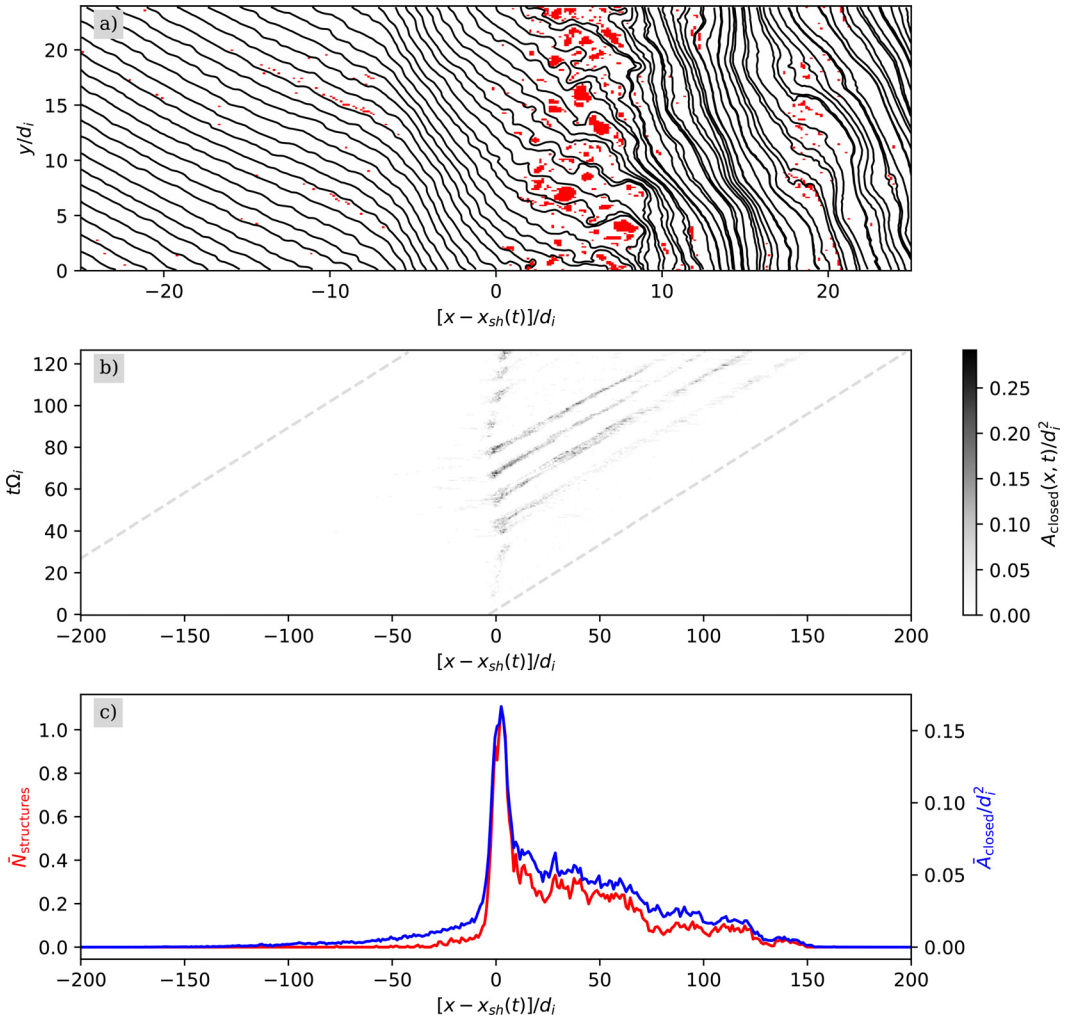

FIG. 2. An example of the quantification of closed field area within quasi-parallel shock simulation U6T40, showing (a) the magnetic field lines (black) and closed field regions (red) at $t\Omega_i = 125$ for the region close to the shock ramp, (b) time-dependence of the total closed field area $A_{\mathrm{closed}}(x,t)$ at a given distance from the shock, and (c) average across all times of the closed field area $\bar{A}_{\mathrm{closed}}(x)$ (blue) and number of distinct closed field structures $\bar{N}_{\mathrm{structures}}$ (red). The dashed lines in panel (b) represent the inflow and reflecting boundaries.

approaches within $50d_i$ of the upstream boundary. For both measures, we identify a small rise in the upstream, followed by a sharp peak in the shock ramp, followed by a gradual decay downstream.

C. Parametric dependence

Here, we examine the differences in reconnection observed across each of the simulations included in this study, quantified by the area of closed magnetic field regions as described in Sec. III B. Figure 3 shows the peak closed field area across all times for each of the simulations, organized according to the Alfvén Mach number M_A and shock orientation θ_{Bn}. We find, broadly, that the peak area of closed field regions increases with Mach number and decreases with θ_{Bn}, and that quasi-perpendicular shocks exhibit typically an order of magnitude lower peak area than quasi-parallel shocks of similar Mach number. However, we note that for the smallest Mach number simulation U2T10, which is very close to the boundary between sub- and supercritical shocks, we do not observe the growth of waves in the foot due to the ion–ion beam instability. This results in the lowest closed field area among all simulations.

We examine how the closed field area $\bar{A}_{\mathrm{closed}}(x)$ varies with distance from the shock for several simulations in Fig. 4. Each of these plots takes the same form as the blue line in panel (c) of Fig. 2. Panel (a) of Fig. 4 shows the spatial dependence of closed field area for simulations initialized with inflow velocity $U_0/V_A = 6$, such that $M_A \approx 8$. Hence, differences arise chiefly from the changes in the shock orientation θ_{Bn}. Most clearly, the closed field area is negligible for simulations with $\theta_{Bn} > 45°$. This indicates that reconnection is not occurring for quasi-perpendicular shocks in this parameter regime, resulting in no change of magnetic topology.

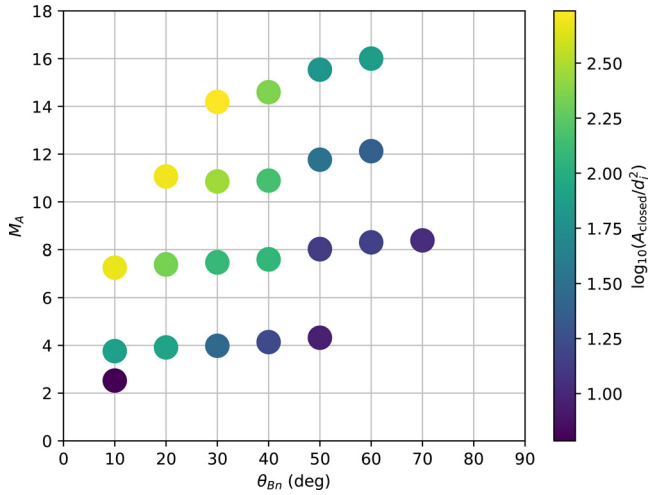

FIG. 3. The peak total area of closed field regions across all times for each simulation, as a function of shock orientation θ_{Bn} and Mach number M_A.

As the angle θ_{Bn} is reduced, we observe a gradual increase in the closed field area upstream of the shock ramp, consistent with more parallel shocks generating a more disordered or turbulent foreshock and foot. However, for shocks that exhibit non-negligible reconnection (i.e., for quasi-parallel shocks, $\theta_{Bn} < 45°$), we see weak or no dependence of the closed field area on θ_{Bn} in the region downstream of the shock ramp.

Panel (b) of Fig. 4 demonstrates the spatial dependence of closed field area for simulations with $\theta_{Bn} = 30°$, varying only the Mach number M_A. In these cases, increasing the Mach number appears to increase the closed field area at all distances from the shock ramp. This indicates that increasing the Mach number results in more significant changes to the local magnetic topology by reconnection, consistent with the larger amplitude fluctuations seen in the right column of Fig. 1. We also note that increasing the Mach number appears to result in closed field regions persisting further downstream of the shock. However, the effect appears to be diminishing for the highest Mach numbers.

D. Downstream decay

In order to quantitatively compare the decay rate of the closed field area downstream of each shock, we fit a function of the form

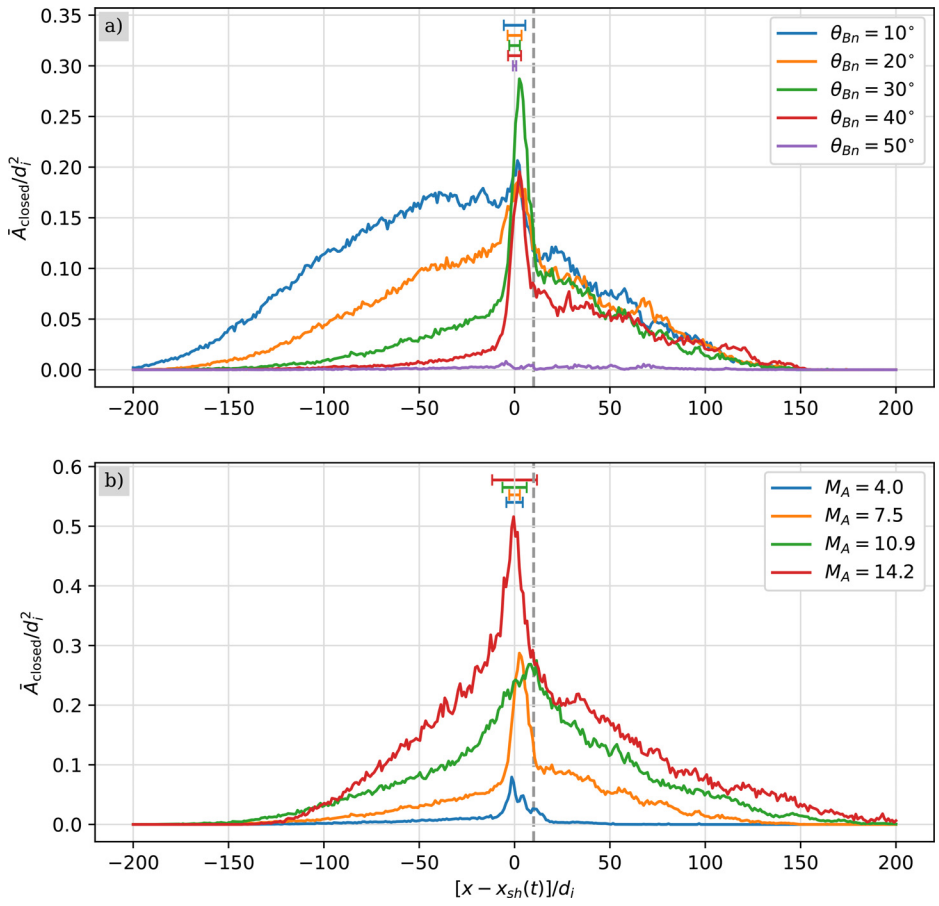

FIG. 4. The number of closed-field cells as a function of distance from the shock, as in panel (c) of Fig. 2, for shock simulations of different parameters. Panel (a) shows dependence on shock orientation θ_{Bn} for Mach number $M_A \approx 8$, while panel (b) shows dependence on M_A for $\theta_{Bn} = 30°$. The gray dashed line marks the boundary for the function fitting discussed in Sec. III D. Results for simulations with $\theta_{Bn} = 60°$, 70° would closely overlay the result for $\theta_{Bn} = 50°$ in panel (a), and are therefore not shown to preserve clarity. Error bars at the top of each panel depict the standard deviation of the position of the shock ramp from $[x - x_{sh}] = 0$ as a result of shock nonstationarity (e.g., cyclic reformation).

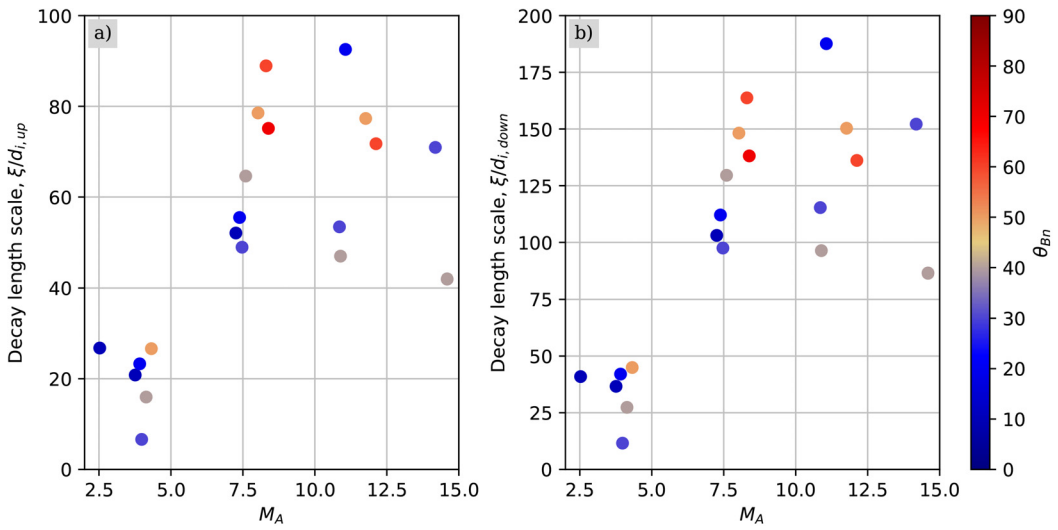

FIG. 5. Parametric dependence of the decay length scale ξ of the closed-field area downstream of the shock, from a fit of the form $A_{\text{closed}} \propto e^{-(x-x_{sh})/\xi}$ for $x - x_s(t) > 10d_i$. Panel (a) gives the decay scale normalized to the upstream ion inertial length $d_{i,up}$ in the solar wind, while panel (b) gives the decay scale normalized to the mean of the downstream ion inertial length $d_{i,down}$ in the magnetosheath. The color represents the shock orientation θ_{Bn}, where quasi-parallel shocks are shown in blue and quasi-perpendicular shocks in red.

$\bar{A}_{\text{closed}} \propto e^{-(x-x_{sh})/\xi}$ in the region $x - x_{sh} > 10d_i$. This region is bounded by the gray dashed line in Fig. 4. The decay scale length ξ for each simulation is shown in Fig. 5. The shock orientation θ_{Bn} is also shown for each simulation in color, with quasi-perpendicular shocks shown in red, and quasi-parallel shocks shown in blue. We find that for the lowest Mach number shocks with $M_A < 5$, the decay rate appears significantly higher, with a scale length $\xi \approx 25d_{i,up}$ or $50d_{i,down}$. This difference is also apparent in the lower panel of Fig. 4. Disregarding quasi-perpendicular shocks, for which we do not observe significant signatures of reconnection, we confirm for $M_A > 5$ that there is no clear dependence of the decay rate on θ_{Bn} and only weak dependence on Mach number M_A. For all cases with $M_A \sim 8$ and for all but two cases with greater Mach number, we observe a scale length of $\xi \approx 50d_{i,up}$ or $100d_{i,down}$. For a typical ion inertial length of $d_i \approx 50$ km in the magnetosheath, we therefore expect decay of shock-driven reconnected (closed-field) structure to occur over a scale of approximately an Earth radius, R_E. We note that the width of the magnetosheath is typically on the order of 1–3 R_E at the subsolar point. This implies that we expect the remnants of shock-driven reconnection to be observed throughout the dayside magnetosheath.

E. Structure distributions

Finally, we examine the distribution of the properties of closed field structures generated at the shock. Figure 6 shows the distribution of individual structure areas A' and enclosed magnetic flux Φ as a function of distance from the shock. The magnetic flux is derived from $\Phi = \sum_i B_{z,i}\Delta x^2$, where the sum over each grid cell i is performed for each cell in the closed field area A'. The position recorded in the distributions in Fig. 6 is that of the furthest upstream grid cell included within each distinct closed field region. We also note that since these distributions include all available time steps, each structure's full trajectory is included in the distribution. Figure 6 shows the results for simulation U6T30 with $M_A = 7.5$ and $\theta_{Bn} = 30°$. The features discussed below are typical of the quasi-parallel simulations with $M_A > 5$.

From panel (a) of Fig. 6, we find that smaller closed field structures are more common than larger structures throughout the full range of distances from the shock. However, the largest structures are observed first at the shock ramp, and decay downstream along with the total closed field area (as seen in Figs. 2 and 4).

Panel (b) of Fig. 6 shows the distribution of the magnetic flux contained within each closed field structure. By comparing the distributions in both panels (a) and (b), we find that the upstream population of closed field structures carries disproportionately less flux relative to their size. This is due to the relatively small out-of-plane magnetic field B_z in the upstream region, as seen in Fig. 1. Furthermore, we find that the flux distributions are approximately symmetric; similar distributions of positive and negative magnetic flux are seen at all distances. Although it appears there may be a small excess of structures with the highest, positive flux $\Phi/(B_0 d_i^2) \approx +10$ close to the ramp, this bias is not reflected in the other simulations presented in this paper (not shown). Indeed, for other cases in Table I with similar shock parameters, we see similar bias toward negative flux, or no clear bias at all.

IV. CONCLUSIONS

Here, we have performed a series of 2.5D hybrid (kinetic ion, fluid electron) particle-in-cell simulations of collisionless shock waves, over a range of shock parameters typical of Earth's bow shock. These simulations display a number of ion-scale kinetic processes within the shock layer, including cyclic reformation, ripples, and magnetic reconnection within a disordered or turbulent transition region. For the simulations described here, reconnection is caused by the wave growth associated with the non-resonant ion–ion beam instability in the upstream region, as seen by Gingell *et al.*[14] and more fully described

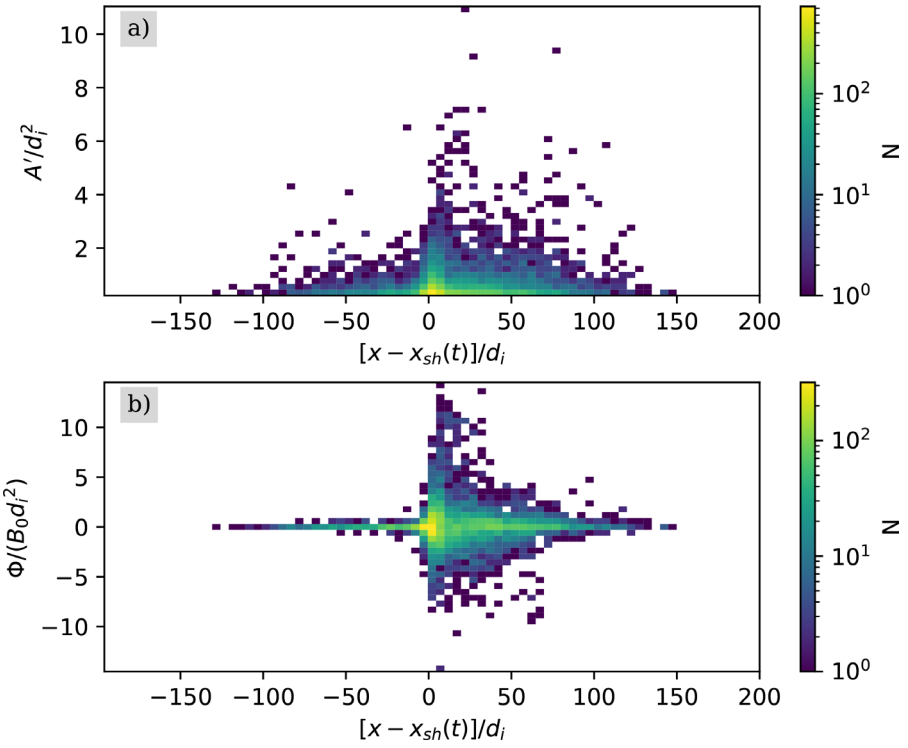

FIG. 6. Distribution of closed field structures with (a) a given area A' and (b) magnetic flux Φ, as a function of position $x - x_{sh}(t)$ according to their furthest upstream cell relative to the shock ramp. The distributions are given for simulation U6T30 with Mach number $M_A = 7.5$ and $\theta_{Bn} = 30^\circ$. The number N (shown in color) represents the number of distinct closed field structures with the given location, area and magnetic flux.

by Bessho *et al.*[16] In order to assess the prevalence of magnetic reconnection, we have quantified the number and area of "closed magnetic field" structures and examined how these structures vary with both distance from the shock and with different shock parameters.

We note several key findings from examining the set of 22 simulations. First, significant magnetic reconnection occurs only for supercritical, quasi-parallel shocks. While some case studies of magnetosheath crossings by Magnetospheric Multiscale have shown that thin current sheets (and hence magnetic reconnection) may be more common in the magnetosheath downstream of quasi-parallel shocks,[29,30] a broad survey of actively reconnecting current sheets associated with the shock transition region has shown that reconnection may be a universal feature, with only weak dependence on shock parameters.[9] Similar trends have also been seen further downstream in the magnetosheath.[10] That we do not see any significant evidence of reconnection in quasi-perpendicular shocks in this study is likely indicative of the chosen initial conditions. For example, all simulations described in this study have $\beta = 1$, whereas reconnection at quasi-perpendicular shocks may arise only for low beta plasmas[19] or very high Mach number shocks.[12] Furthermore, the chosen model imposes further restrictions: fully 3D simulations and those which enable physics on the electron kinetic scales may allow for the growth of additional plasma instabilities. Hence, the results here must be interpreted as narrowly targeted, exploring principally the influence of the non-resonant ion–ion beam instability described by Bessho *et al.*[16] With that in mind, we find that the peak closed field area in the simulations (and hence the amount of reconnected flux) increases with the Mach number and decreases with shock orientation θ_{Bn}.

In examining the spatial dependence of the number of closed-field structures and their area, we find that reconnection is most prevalent in a thin layer ($\approx 10 d_i$) surrounding the shock ramp. Downstream, the number of closed-field structures and the total closed field area decay over a length scale of approximately $50 d_i$. Perhaps the most interesting finding of this study is that the decay rate of the closed field area is not strongly affected by the upstream shock parameters for quasi-parallel shocks above $M_A \approx 5$. Therefore, we may expect to see similar numbers of thin current sheets downstream of the shock for all quasi-parallel shocks which exhibit the non-resonant ion–ion beam instability described above. This is consistent with a survey of the prevalence of thin current sheets in the magnetosheath, for which Gingell *et al.*[10] observed weak or no dependence of the number density of current sheets on upstream parameters.

An examination of the distribution of structure sizes and magnetic flux within the closed field regions has revealed that the largest structures are localized to the shock ramp and that closed-field structures in the upstream carry proportionally less magnetic flux than those in the downstream region.

In summary, we have shown that the non-resonant ion–ion beam instability of back-streaming ions in the transition region of quasi-parallel shocks can generate reconnecting structures that survive through the shock ramp and into the downstream magnetosheath, with a typical decay scale on the order of $\approx 50 d_i$ or $\approx 1 R_E$. For quasi-parallel shocks with $\beta \approx 1$ and $M_A \leq 14$, this decay rate is not strongly dependent on shock parameters. Future parameteric explorations of the prevalence of reconnection and reconnected structures will require three-dimensional or fully-kinetic particle-in-cell models to capture a more comprehensive family of shock processes.

ACKNOWLEDGMENTS

I. Gingell was supported by the Royal Society University Research Fellowship No. URF\R1\191547. This study is also supported by NASA Award No. 80NSSC19K0849. The EPOCH code used in this work was in part funded by the UK EPSRC Grant Nos. EP/G054950/1, EP/G056803/1, EP/G055165/1, EP/M022463/1, and EP/P02212X/1. The research at LASP was supported by NASA Grant Nos. NNG04EB99C, 80NSSC19K0849, and 80NSSC20K0688. L.J.F. and J.P. were supported by the UK's Science and Technology Facilities Council (STFC) through Studentship Nos. ST/T506424/1 (2279917) and ST/V507064/1 (2502298).

AUTHOR DECLARATIONS

Conflict of Interest

The authors have no conflicts to disclose.

Author Contributions

Imogen Gingell: Conceptualization (lead); Formal analysis (lead); Methodology (lead); Project administration (equal); Writing – original draft (lead); Writing – review & editing (lead). **Steve Schwartz:** Conceptualization (supporting); Writing – review & editing (supporting). **Harald Kucharek:** Conceptualization (supporting); Project administration (equal); Writing – review & editing (supporting). **Charlie J. Farrugia:** Conceptualization (supporting); Writing – review & editing (supporting). **Laura J. Fryer:** Conceptualization (supporting); Writing – review & editing (supporting). **James Plank:** Conceptualization (supporting); Writing – review & editing (supporting). **Karlheinz J. Trattner:** Conceptualization (supporting); Writing – review & editing (supporting).

DATA AVAILABILITY

The data that support the findings of this study are available from the corresponding author upon reasonable request.

REFERENCES

[1]D. Burgess and M. Scholer, *Collisionless Shocks in Space Plasmas* (Cambridge University Press, 2015).
[2]P. L. Auer, H. Hurwitz, Jr., and R. W. Kilb, "Large-amplitude magnetic compression of a collision-free plasma. II. Development of a thermalized plasma," Phys. Fluids **5**, 298–316 (1962).
[3]J. T. Gosling and A. E. Robson, "Ion reflection, gyration, and dissipation at supercritical shocks," Am. Geophys. Union Geophys. Monogr. Ser. **35**, 141–152 (1985).
[4]D. L. Morse, W. W. Destler, and P. L. Auer, "Nonstationary behavior of collisionless shocks," Phys. Rev. Lett. **28**, 13–16 (1972).
[5]I. Gingell, S. J. Schwartz, J. P. Eastwood, J. L. Burch, R. E. Ergun, S. Fuselier, D. J. Gershman, B. L. Giles, Y. V. Khotyaintsev, B. Lavraud, P.-A. Lindqvist, W. R. Paterson, T. D. Phan, C. T. Russell, J. E. Stawarz, R. J. Strangeway, R. B. Torbert, and F. Wilder, "Observations of magnetic reconnection in the transition region of quasi-parallel shocks," Geophys. Res. Lett. **46**, 1177–1184, https://doi.org/10.1029/2018GL081804 (2019).
[6]S. Wang, L.-J. Chen, N. Bessho, M. Hesse, L. B. Wilson, B. Giles, T. E. Moore, C. T. Russell, R. B. Torbert, and J. L. Burch, "Observational evidence of magnetic reconnection in the terrestrial bow shock transition region," Geophys. Res. Lett. **46**, 562–570, https://doi.org/10.1029/2018GL080944 (2019).
[7]T. D. Phan, J. P. Eastwood, M. A. Shay, J. F. Drake, B. U. Ö. Sonnerup, M. Fujimoto, P. A. Cassak, M. Øieroset, J. L. Burch, R. B. Torbert, A. C. Rager, J. C. Dorelli, D. J. Gershman, C. Pollock, P. S. Pyakurel, C. C. Haggerty, Y. Khotyaintsev, B. Lavraud, Y. Saito, M. Oka, R. E. Ergun, A. Retino, O. L. Contel, M. R. Argall, B. L. Giles, T. E. Moore, F. D. Wilder, R. J. Strangeway, C. T. Russell, P. A. Lindqvist, and W. Magnes, "Electron magnetic reconnection without ion coupling in Earth's turbulent magnetosheath," Nature **557**, 202–206 (2018).
[8]J. E. Stawarz, J. P. Eastwood, T. D. Phan, I. L. Gingell, M. A. Shay, J. L. Burch, R. E. Ergun, B. L. Giles, D. J. Gershman, O. L. Contel, P.-A. Lindqvist, C. T. Russell, R. J. Strangeway, R. B. Torbert, M. R. Argall, D. Fischer, W. Magnes, and L. Franci, "Properties of the turbulence associated with electron-only magnetic reconnection in Earth's magnetosheath," Astrophys. J. Lett. **877**, L37 (2019).
[9]I. Gingell, S. J. Schwartz, J. P. Eastwood, J. E. Stawarz, J. L. Burch, R. E. Ergun, S. A. Fuselier, D. J. Gershman, B. L. Giles, Y. V. Khotyaintsev, B. Lavraud, P. A. Lindqvist, W. R. Paterson, T. D. Phan, C. T. Russell, R. J. Strangeway, R. B. Torbert, and F. Wilder, "Statistics of reconnecting current sheets in the transition region of Earth's bow shock," J. Geophys. Res. **125**, e27119, https://doi.org/10.1029/2019JA027119 (2020).
[10]I. Gingell, S. J. Schwartz, H. Kucharek, C. J. Farrugia, and K. J. Trattner, "Observing the prevalence of thin current sheets downstream of Earth's bow shock," Phys. Plasmas **28**, 102902 (2021).
[11]S. J. Schwartz, H. Kucharek, C. J. Farrugia, K. Trattner, I. Gingell, R. E. Ergun, R. Strangeway, and D. Gershman, "Energy conversion within current sheets in the Earth's quasi-parallel magnetosheath," Geophys. Res. Lett. **48**, e2020GL091859, https://doi.org/10.1029/2020GL091859 (2021).
[12]Y. Matsumoto, T. Amano, T. N. Kato, and M. Hoshino, "Stochastic electron acceleration during spontaneous turbulent reconnection in a strong shock wave," Science **347**, 974–978 (2015).
[13]T. Nishigai and T. Amano, "Mach number dependence of ion-scale kinetic instability at collisionless perpendicular shock: Condition for Weibel-dominated shock," Phys. Plasmas **28**, 072903 (2021).
[14]I. Gingell, S. J. Schwartz, D. Burgess, A. Johlander, C. T. Russell, J. L. Burch, R. E. Ergun, S. Fuselier, D. J. Gershman, B. L. Giles, K. A. Goodrich, Y. V. Khotyaintsev, B. Lavraud, P.-A. Lindqvist, R. J. Strangeway, K. Trattner, R. B. Torbert, H. Wei, and F. Wilder, "MMS observations and hybrid simulations of surface ripples at a marginally quasi-parallel shock," J. Geophys. Res. **122**, 11, https://doi.org/10.1002/2017JA024538 (2017).
[15]N. Bessho, L.-J. Chen, S. Wang, M. Hesse, and L. B. Wilson III, "Magnetic reconnection in a quasi-parallel shock: Two-dimensional local particle-in-cell simulation," Geophys. Res. Lett. **46**, 9352–9361, https://doi.org/10.1029/2019GL083397 (2019).
[16]N. Bessho, L.-J. Chen, S. Wang, M. Hesse, L. B. Wilson, and J. Ng, "Magnetic reconnection and kinetic waves generated in the Earth's quasi-parallel bow shock," Phys. Plasmas **27**, 092901 (2020).
[17]N. Bessho, L.-J. Chen, J. E. Stawarz, S. Wang, M. Hesse, L. B. Wilson, and J. Ng, "Strong reconnection electric fields in shock-driven turbulence," Phys. Plasmas **29**, 042304 (2022).
[18]J. Ng, L.-J. Chen, N. Bessho, J. Shuster, B. Burkholder, and J. Yoo, "Electron-scale reconnection in three-dimensional shock turbulence," Geophys. Res. Lett. **49**, e2022GL099544, https://doi.org/10.1029/2022GL099544 (2022).
[19]Q. Lu, Z. Yang, H. Wang, R. Wang, K. Huang, S. Lu, and S. Wang, "Two-dimensional particle-in-cell simulation of magnetic reconnection in the downstream of a quasi-perpendicular shock," Astrophys. J. **919**, 28 (2021).
[20]D. Winske and K. B. Quest, "Magnetic field and density fluctuations at perpendicular supercritical collisionless shocks," J. Geophys. Res. **93**, 9681–9693, https://doi.org/10.1029/JA093iA09p09681 (1988).
[21]A. P. Matthews, "Current advance method and cyclic leapfrog for 2D multispecies hybrid plasma simulations," J. Comput. Phys. **112**, 102–116 (1994).
[22]T. D. Arber, K. Bennett, C. S. Brady, A. Lawrence-Douglas, M. G. Ramsay, N. J. Sircombe, P. Gillies, R. G. Evans, H. Schmitz, A. R. Bell, and C. P. Ridgers, "Contemporary particle-in-cell approach to laser-plasma modelling," Plasma Phys. Controlled Fusion **57**, 113001 (2015).
[23]S. P. Gary, "Electromagnetic ion/ion instabilities and their consequences in space plasmas: A review," Space Sci. Rev. **56**, 373–415 (1991).
[24]R. E. Lowe and D. Burgess, "The properties and causes of rippling in quasi-perpendicular collisionless shock fronts," Ann. Geophys. **21**, 671–679 (2003).
[25]A. Johlander, S. J. Schwartz, A. Vaivads, Y. V. Khotyaintsev, I. Gingell, I. B. Peng, S. Markidis, P.-A. Lindqvist, R. E. Ergun, G. T. Marklund, F. Plaschke,

W. Magnes, R. J. Strangeway, C. T. Russell, H. Wei, R. B. Torbert, W. R. Paterson, D. J. Gershman, J. C. Dorelli, L. A. Avanov, B. Lavraud, Y. Saito, B. L. Giles, C. J. Pollock, and J. L. Burch, "Rippled quasiperpendicular shock observed by the magnetospheric multiscale spacecraft," Phys. Rev. Lett. **117**, 165101 (2016).

[26]A. Johlander, A. Vaivads, Y. V. Khotyaintsev, I. Gingell, S. J. Schwartz, B. L. Giles, R. B. Torbert, and C. T. Russell, "Shock ripples observed by the MMS spacecraft: Ion reflection and dispersive properties," Plasma Phys. Controlled Fusion **60**, 125006 (2018).

[27]S. J. Schwartz and D. Burgess, "Quasi-parallel shocks: A patchwork of three-dimensional structures," Geophys. Res. Lett. **18**, 373–376, https://doi.org/10.1029/91GL00138 (1991).

[28]A. Johlander, M. Battarbee, L. Turc, U. Ganse, Y. Pfau-Kempf, M. Grandin, J. Suni, V. Tarvus, M. Bussov, H. Zhou, M. Alho, M. Dubart, H. George, K. Papadakis, and M. Palmroth, "Quasi-parallel shock reformation seen by magnetospheric multiscale and ion-kinetic simulations," Geophys. Res. Lett. **49**, e2021GL096335, https://doi.org/10.1029/2021GL096335 (2022).

[29]E. Yordanova, Z. Vörös, A. Varsani, D. B. Graham, C. Norgren, Y. V. Khotyaintsev, A. Vaivads, E. Eriksson, R. Nakamura, P. A. Lindqvist, G. Marklund, R. E. Ergun, W. Magnes, W. Baumjohann, D. Fischer, F. Plaschke, Y. Narita, C. T. Russell, R. J. Strangeway, O. L. Contel, C. Pollock, R. B. Torbert, B. J. Giles, J. L. Burch, L. A. Avanov, J. C. Dorelli, D. J. Gershman, W. R. Paterson, B. Lavraud, and Y. Saito, "Electron scale structures and magnetic reconnection signatures in the turbulent magnetosheath," Geophys. Res. Lett. **43**, 5969–5978, https://doi.org/10.1002/2016GL069191 (2016).

[30]E. Yordanova, Z. Vörös, S. Raptis, and T. Karlsson, "Current sheet statistics in the magnetosheath," Front. Astron. Space Sci. **7**, 00002 (2020).